Dalton Transactions

ROYAL SOCIETY OF CHEMISTRY

PAPER

View Article Online
View Journal

Cite this: DOI: 10.1039/d2dt00770c

Flexible translucent persistent luminescent films based on $Sr_2MgSi_2O_7:Eu^{2+},Dy^{3+}$ cellulose ether composites†

Douglas L. Fritzen, [a] Elaine A. de Mattos, [a] Denise F. S. Petri, [a] Verônica C. Teixeira, [b] Everton Bonturim [c] and Lucas C. V. Rodrigues *[a]

Received 10th March 2022,
Accepted 24th May 2022

DOI: 10.1039/d2dt00770c

rsc.li/dalton

Persistent luminescent materials are present in several recent studies on new applications and novel properties. In this work, we demonstrate, for the first time, the production of translucent flexible persistent composites based on $Sr_2MgSi_2O_7:Eu^{2+},Dy^{3+}$ (SMSO) into cellulose ether matrix film. The composite was successfully prepared through a new optimized route of co-precipitation and microwave-assisted annealing followed by (3-aminopropyl)triethoxysilane (APTES) coating and dispersion in hydroxypropyl methylcellulose (HPMC). The SMSO@APTES/HPMC films show persistent luminescence emission at 475 nm (blue) and high transmittance in the visible range. To understand the fine distribution of the nanoparticles in the matrix, we have investigated their structure and dispersion by using Synchrotron Radiation X-ray fluorescence mapping and Scanning Transmission X-ray Microscopy. This innovative composite could bring new perspectives for the class of persistent luminescence materials, enhancing technologies in progress throwing light on new applications never perceived.

1. Introduction

The persistent luminescence phenomenon, in which light energy is stored in a solid-inorganic material, might be known mainly for its glow-in-the-dark characteristics, but it is much more complex than the visual charm. In this phenomenon, during irradiation (*e.g.*, sunlight, UV, X-ray, *etc.*), the material's charge carriers (electron or holes) are trapped in defects. The stored energy is then released under a thermal stimulus, which bleaches the defects, resulting in persistent light emission that can last for minutes, hours, or days.[1–5]

Since the re-discovery of the phenomenon by Matsuzawa *et al.* in 1996[6] and the synthesis of $SrAl_2O_4:Eu^{2+},Dy^{3+}$ green-emission crystals, new materials have been designed and developed with different emission centers, emission wavelengths, and afterglow endurance.[7–9] The most common and well-known applications for this phenomenon are signalization (safety and exit signs) and decoration. Poelman *et al.*[10] reported a recent review that summarizes several applications that are either currently applied or are promising and considered challenges. Amongst these applications, persistent luminescent materials are promising to be used on extreme-condition thermometers, AC LEDs, road marking, solar energy harvesting solutions, photocatalysis, and bio-applications (bioimaging and phototherapy).[9–11]

The progress of new applications based on Persistent Luminescent Materials (PLM) depends highly on the development of new materials with specific characteristics, such as particle size (*e.g.*, bio-applications), chemical resistance (*e.g.*, energy harvesting), and bright emission that could be perceived by the human eye (*e.g.*, safety signs).[7–12] With that in mind, the development of new translucent/transparent PLM would bring light to current application researches, facilitate the development of challenging applications, and possibly open the doors for new ideas in this research field. However, the production of translucent materials requires particles with homogeneous dimensions in the nanoscale in order to diminish the light scattering phenomenon. The main challenge in synthesizing persistent nanomaterials is that, in order to thermodynamically favor the defect formation and the creation of a proper crystalline field and phase, high temperatures are required, which leads to sintering of the powdery materials. Besides, PLM based on Eu^{2+} ions require a strong reducing environment, which normally is achieved with reducing atmos-

[a]Department of Fundamental Chemistry, Institute of Chemistry, University of São Paulo, 05508-000 São Paulo-SP, Brazil. E-mail: lucascvr@iq.usp.br
[b]Brazilian Synchrotron Light Laboratory (LNLS), Brazilian Center for Research in Energy and Materials (CNPEM), 13083-970 Campinas, SP, Brazil
[c]Department of Chemistry, School of Engineering, Mackenzie Presbyterian University, 01302-907 São Paulo-SP, Brazil

†Electronic supplementary information (ESI) available: XRD, FTIR, synchrotron STXM and XRF nanomapping, HPMC excitation and emission spectra. See DOI: https://doi.org/10.1039/d2dt00770c

pheres at high temperatures. For example, the reduction process of Eu^{2+} in $Sr_2MgSi_2O_7$ with 5% CO atmosphere is efficient only at temperatures above 900 °C.[13]

Translucent and flexible persistent luminescent materials are seldom reported in the literature. Considering that, this study presents a new translucent persistent luminescent composite based on $Sr_2MgSi_2O_7$:Eu^{2+},Dy^{3+} (SMSO) and hydroxypropyl methylcellulose (HPMC). The narrow size distribution of SMSO particles prevented the film from becoming opaque. Due to the unprecedent characteristics of these materials, opacity, persistent luminescence time and Synchrotron Radiation X-ray fluorescence nanomapping analyses allowed better understanding of the composites' characteristics.

2. Experimental section

2.1. $Sr_2MgSi_2O_7$:Eu^{2+},Dy^{3+} nanoparticle synthesis

To obtain the SMSO nanoparticles, a co-precipitation method of synthesis was carried out. $Sr(NO_3)_2$ (Sigma Aldrich 99.99%), $MgCl_2$ (Sigma Aldrich 99.99%), Eu_2O_3 (99.999% Quingdao Xinguanya Mining Industry Co.), Dy_2O_3 (99.999% Quingdao Xinguanya Mining Industry Co.), and Na_2SiO_3 (99.99% Merck) were used as starting materials. $Eu(NO_3)_3$ and $Dy(NO_3)_3$ solutions were prepared using concentrated HNO_3 and distilled water. Then, 25 mL of an aqueous solution containing the cations of interest was obtained by mixing $Sr(NO_3)_2$ (63 mmol L^{-1}), $MgCl_2$ (33 mmol L^{-1}), $Eu(NO_3)_3$ (0.7 mmol L^{-1}), and $Dy(NO_3)_3$ (2.8 mmol L^{-1}). The solution was added dropwise (at a rate of 1 drop per second) into the precipitant solution (25 mL Na_2SiO_3 0.1 mol L^{-1}) at room temperature, under vigorous stirring. The obtained solid was then centrifuged for 5 min under 9000 rpm and washed several times with EtOH/H_2O (1 : 1) solution to remove the excess of soluble nitrates, chlorides, and silicates. The precipitate was dried at 100 °C in a laboratory drying oven for 2 hours and then heated in a microwave oven for 30 min at 1000 W, which leads to temperatures close to 1200 °C.[13] Activated carbon was used as microwave susceptor to generate heat and produce a local reducing CO(g) atmosphere. This reducing atmosphere is provided to obtain Eu^{2+} from the oxidized state of Eu^{3+}. A full schematic setup of the microwave setting used can be found in the work of Merízio *et al.*[13]

APTES coating was applied by adding 400 μL of (3-aminopropil) triethoxysilane (APTES) in a suspension containing SMSO (100 mg) in ethanol (10 mL). This mixture was stirred for 24 h at room temperature. APTES is known to create silica-like shells with terminal amino-groups on the oxide surface, improving the dispersibility of the particles while protecting them from water, without quenching the luminescence properties.[14] After the stirring period, the SMSO@APTES solids were dried under vacuum at room temperature.

2.2. Preparation of SMSO@APTES/HPMC thin films

For the preparation of the films, different amounts of SMSO@APTES (0, 1, 5, 10, 50, or 100 mg) were added to 5 mL of 10 g L^{-1} HPMC solution. The mixture was vigorously stirred at room temperature for 30 min, cooled at 5 °C and kept at this temperature for 1 hour. Cooling process is needed to eliminate the air bubbles formed during the dispersion. The solution was cast on a circle-shaped silicone rubber mold. The films were finally obtained after 24 h drying at 50 °C (Fig. 1).[15] The amount of SMSO@APTES in the films was normalized by the area of the substrate (10 cm^2), resulting in films with nominal SMSO concentration of 0, 1, 5, 10, 50, and 100 g m^{-2}.

2.3. Characterization

X-ray diffraction of the obtained SMSO@APTES material was carried out in a Bragg–Brentano XRD (Brucker D2 PHASER) using Cu Kα radiation (λ = 1.5406 Å) in the range of 10–60° (2θ), integration of one second for each 0.5° step. Fourier-Transformed Infrared (FTIR) spectra were measured within the 4000 to 650 cm^{-1} wavenumber range using a Cary 630 (Agilent) spectrometer coupled with the ATR module. The ATR detection diamond was cleaned with 100% v/v isopropanol, and background spectra were registered before every acquisition. SEM images were captured by a JEOL JSM-740 1F Field Emission Scanning Electron Microscope. Emission, excitation, and persistent luminescent spectra were registered in an Edinburgh FLS 980 at room temperature, using a 450 W Xe-lamp as irradiation source. Transmittance spectra of SMSO/HPMC films were carried out in a Shimadzu UV-1601PC spectrophotometer, ranging from 200 to 800 nm at room temperature. The X-ray fluorescence (XRF) mapping and the Scanning Transmission X-Ray Microscopy (STXM) were carried out at the Carnauba beamline from the CNPEM-Sirius Synchrotron facility (Campinas-SP, Brazil). For these measurements, the films were mounted on aluminum frames at room temperature and ambient pressure with excitation energy of 9.656 keV. The STXM was measured using a Photodiode AS04-105A Alibava, and the XRF measurement used a Vortex SDD, 4 elements, Hitachi. The XRF and STXM data were treated using PyMCA as reported by Solé *et al.*[16]

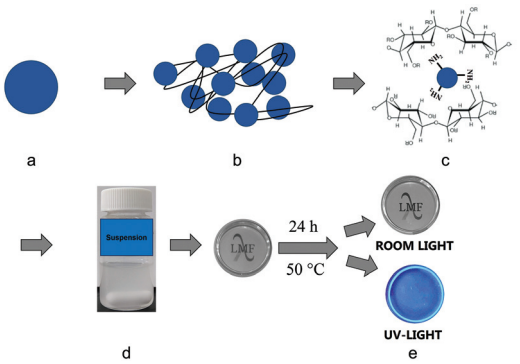

Fig. 1 Schematic diagram of SMSO@APTES thin-film preparation. The steps include (a) the SMSO@APTES particle (blue circle); (b) suspension in HPMC solution; (c) H bond interaction between SMSO@APTES and HPMC; (d) photograph of the suspension SMSO@APTES/HPMC; (e) photographs of the resulting translucent film under room and UV-light.

3. Results

3.1. Composite characterization

The crystalline phase purity of SMSO@APTES was confirmed by XRD measurements, which showed the formation of the expected crystalline phase, $Sr_2MgSi_2O_7$. The presence of the APTES coating did not contribute to the XRD pattern (Fig. S1†). Furthermore, its presence on the particles' surface is demonstrated by the FTIR spectrum, which exhibits a band at 3400 cm^{-1}, typical of NH_2 stretching, indicating that the amine-groups are present after the coating procedure[17–19] (Fig. S2†).

The SMSO@APTES SEM images show well-dispersed particles (Fig. 2a and b) with mean size of 245 ± 84 nm (Fig. 2c). This homogenous distribution without large aggregates is due to the co-precipitation process and the rapid annealing by the microwave process, which avoids significative crystal growth and sintering. This is confirmed by the SEM images of SMSO before microwave (MW) treatment, after MW treatment, and of SMSO@APTES (Fig. S3a–c†). It is observed only a small increase in the mean size with annealing (204 to 245 nm) and nearly no difference with APTES coating (263 nm) (Fig. S3d–f†).

The SMSO@APTES particles stayed well suspended during the time prior to casting the film, even without stirring (Fig. 3a). The cast films showed appreciable flexibility and translucency that visually started to decrease at concentrations higher than 10 g m^{-2}, becoming completely opaque at 100 g m^{-2} (Fig. 3b). Pictures of 1 g m^{-2} (Fig. 3c and d), 10 g m^{-2} (Fig. 3e and f) and 100 g m^{-2} (Fig. 3g and h) films show their translucent and persistent luminescence aspects. One might see that the luminescence also increases visually with the concentration, as expected. The thickness of the films also increases at higher concentrations, ranging from *ca.* 25 μm for the 0–10 g m^{-2} range to 105 μm for the 50–100 g m^{-2} range. This increase happens because the substrate used has a limited area and increasing the total volume (film and particles) leads to a thickness growth.

In order to quantify the translucency, the transmittance spectra of the films, ranging from 200 nm to 800 nm, were registered (Fig. 4a). The mean transmittance values in the visible range (400 nm–700 nm) were calculated and presented in Fig. 4b. The maximum transmittance (80%) of the composite is represented by the curve of 0 g m^{-2} (HPMC pure film).

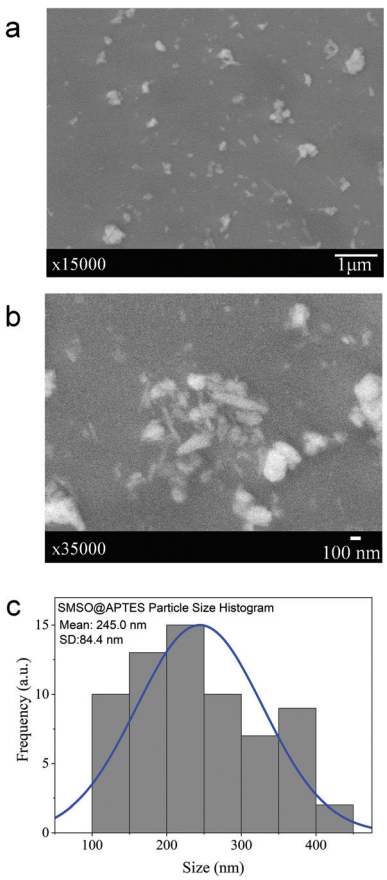

Fig. 2 (a) SEM images of SMSO@APTES particles with ×15 000 magnification and (b) ×35 000 magnification. (c) Histogram for particle size distribution obtained by image analyses using ImageJ software routine.

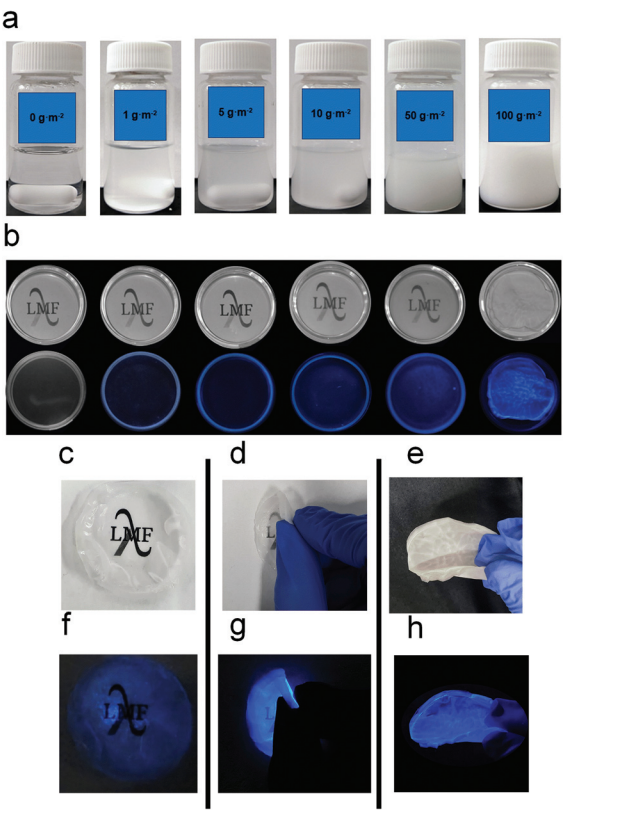

Fig. 3 (a) Images of SMSO@APTES/HPMC suspensions, varying from 0 to 100 g m^{-2}. (b) (upper row) Thin films under room light, (bottom row) thin films under UV-light excitation source (365 nm). Pictures under room light of (c) 1 g m^{-2}, (d) 10 g m^{-2}, and (e) 100 g m^{-2} films. Persistent luminescence of (f) 1 g m^{-2}, (g) 10 g m^{-2}, and (h) 100 g m^{-2} films.

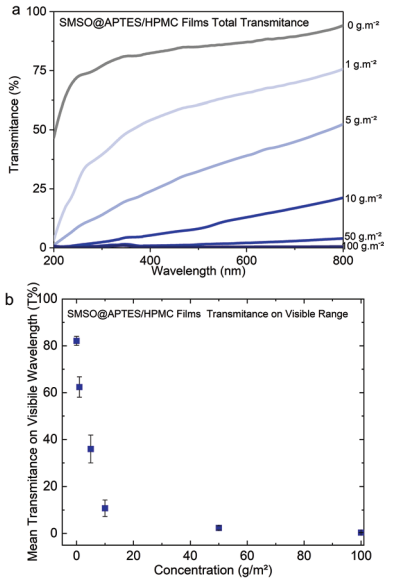

Fig. 4 (a) Total transmittance of SMSO@APTES/HPMC films and (b) mean transmittance for visible wavelength range (400–700 nm) of samples with 0, 1, 5, 10, 50, and 100 g m^{-2} of luminescent nanoparticles.

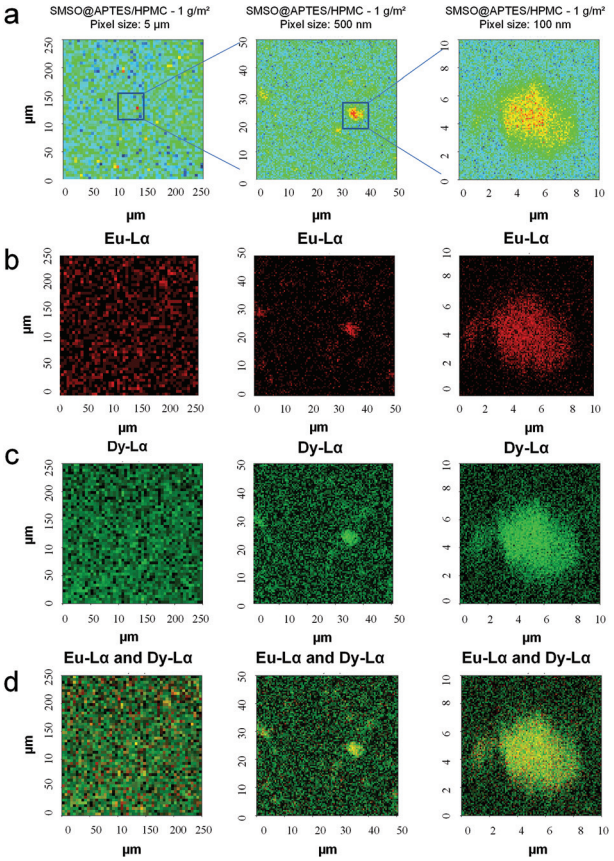

Fig. 5 (a) STXM of SMSO@APTES/HPMC 1 g m^{-2} film at 9.656 keV. (b–d) XRF mapping of SMSO@APTES/HPMC 1 g m^{-2} film at (b) Eu Lα (5.845 keV); (c) Dy Lα (6.495 keV); (d) Eu and Dy Lα lines under 9.656 keV excitation.

The transmittance of the 1 g m^{-2} composite (*ca.* 60%) is close to the pure HPMC film. Increasing the concentration up to 10 g m^{-2} leads to an abrupt decrease of the mean visible transmittance, which reaches its lowest value at the concentration of 100 g m^{-2}, as the material is visually opaque and allows almost no transmittance (0%).

The microscopic study of nanomaterial dispersion in cellulose-based composites is a hard task, as stated by Oksman and Moon,[20] due to the low contrast in TEM images, requiring staining procedures with high atomic number compounds like uranyl acetate. Besides, analyses like SEM and AFM are limited to surface characterization. Scanning Transmission X-Ray Microscopy and X-ray mapping were performed in a 4th generation Synchrotron Radiation facility. This new tool characterizes the distribution and integrity of the nanoparticles within the HPMC matrix, using a monochromatic X-ray beam with 500 × 200 nm spot size. Scanning Transmission X-Ray Microscopy was registered simultaneously with the X-ray Fluorescence mapping (Fig. 5).

The STXM images were registered under irradiation energy of 9.656 keV, which is above the L-edges of the doping ions and Sr, and above K-edge of Al, Si, Mg, and O. The image of the 1 g m^{-2} film in low magnification show a homogeneous absorption all over the film. Since the size of the X-ray beam is close to the size of the nanoparticles, it is only possible to have a good definition of larger structures. At higher magnifications, one can also observe a small aggregate of *ca.* 6 μm size. The formation of aggregates might occur during the film casting, since some water pockets may be created, thus accumulating the nanoparticles which aggregate during the drying process.

X-ray fluorescence mappings (Fig. 5b–d) were created integrating the area of Europium and Dysprosium Lα lines from the XRF spectra in each pixel (Fig. S4†). First, it is observed that the entire film presents a well-distributed signal of Eu and Dy, indicating that most of the nanoparticles are non-aggregated and well dispersed. Even in the higher magnification image (100 nm pixel size), one can observe fluorescence signals homogeneously dispersed in the order of a few pixels around the agglomerate. For the 10 g m^{-2} film (Fig. S5†) a similar aspect is observed with a higher concentration of particles, while for the 100 g m^{-2} (Fig. S6†), the fluorescence signal shows that the nanoparticles occupy almost all the empty film spaces leading to an opaque composite.

The excitation spectra of SMSO and 10 g m^{-2} SMSO@APTES/HPMC composites (Fig. 6) exhibit the broad bands attribute to Eu^{2+} $4f^7(^8S_{7/2}) \rightarrow 4f^6 5d^1(^2D)$ transitions with the maximum at *ca.* 350–360 nm. The film spectrum also exhibits a band at *ca.* 300 nm, similar to the excitation spectrum of the pure HPMC film (Fig. S7†). The emission spectra exhibit the Eu^{2+} $4f^6 5d^1(^2D) \rightarrow 4f^7(^8S_{7/2})$ transitions with the maximum at 475 nm. The narrowed emission band in the composite spectrum might be due to a more rigid environment around

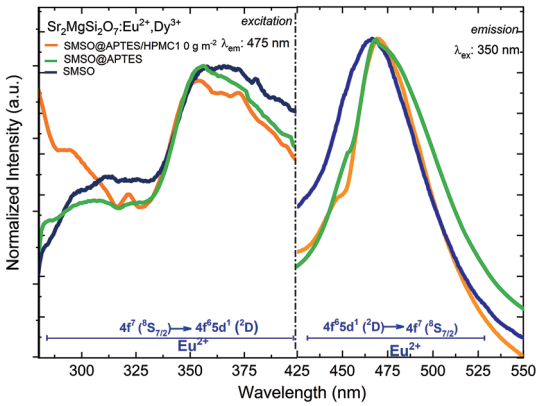

Fig. 6 (left) Excitation spectra of SMSO and SMSO@APTES powders and 10 g m^{-2} SMSO@APTES/HPMC film at room temperature, with emission at 475 nm. (right) Emission spectra of SMSO and SMSO@APTES powders and 10 g m^{-2} SMSO@APTES/HPMC film at room temperature, under 350 nm excitation.

the nanoparticles, leading to smaller vibronic influence on the emission.

The persistent luminescence decay times of the composites (compared to the photomultiplier sensitivity) were measured after 5 min of irradiation at 350 nm, monitoring the emission at 475 nm. In order to compare their persistent times, all measurements were done with the same size of the film sample, and the luminescence was measured until the signal was comparable to the background of the detector (Fig. 7a). The persistent decay time increased with increasing nanoparticle concentration from 0 to 10 g m^{-2}, achieving approximately 90 minutes. This is expected since the absolute number of stored charge carriers is dependent on the mass of the persistent luminescence material.[21] At higher concentrations (50 and 100 g m^{-2}) there is no considerable increase in the decay time, which is possibly caused by shadowing effects when the materials concentration is too high and most of the powder will not be excited, leading to no persistent luminescence, as pointed out by Van der Heggen *et al.*[21] Finally, the persistent luminescence emission spectra is similar for SMSO, SMSO@APTES and SMSO@APTES/HPMC materials (Fig. S8†).

Comparing the persistent luminescence time with the mean opacity in visible range (Fig. 7b) one can observe that they follow similar trends, in which there is a significant increase in the time and the opacity for the films ranging from 0 to 10 g m^{-2}. For higher values there is no significant change on the persistent luminescence duration and the opacity. The small changes in the persistent luminescence decay shapes are mainly due to different amount of stored charge carriers in the films, which influences the intensity *vs.* time curve shape as described earlier by Brito *et al.*[22]

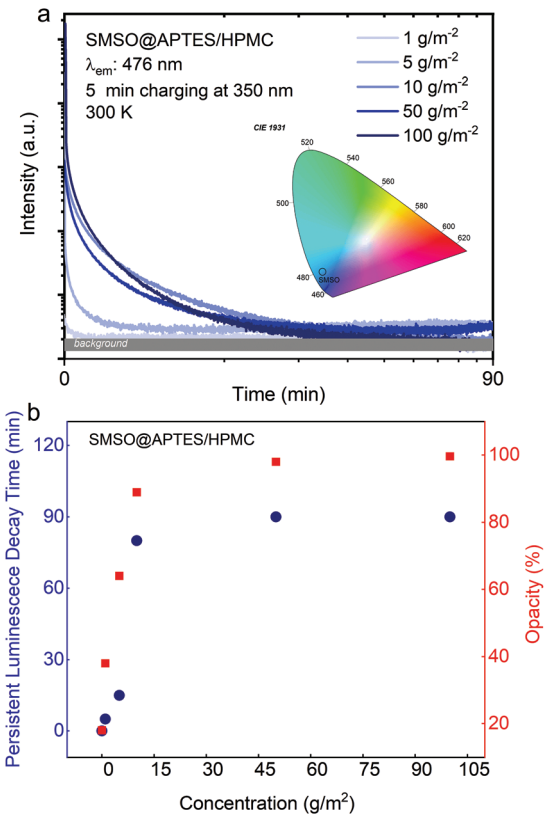

Fig. 7 (a) Persistent Luminescence decay time of SMSO@APTES/HPMC thin films. (b) Relationship between concentration of SMSO on SMSO/HPMC thin film and their persistent luminescent period until fading.

4. Conclusions

In summary, $Sr_2MgSi_2O_7:Eu^{2+},Dy^{3+}$ nanoparticles were successfully obtained through a new route based on co-precipitation with microwave-assisted annealing, and produced the first flexible and translucent persistent composite based on HPMC matrix. The study of the distribution of the nanoparticles in the film was only possible though the use of Synchrotron Carnauba beamline techniques, STXM and XRF mapping. Upon UV-light irradiation, the SMSO@APTES/HPMC films presented a bright blue emission, which lasted for approximately 90 minutes after ceasing the irradiation source on the 10 g m^{-2} composition. Notably, increasing the concentration of nanomaterials on the composites extended the afterglow duration with the drawback of increasing the opacity of the film. The 10 g m^{-2} composition showed an enduring persistency with an appreciable transmittance in the visible range. Therefore, this proof of concept to produce translucent persistent films represents a promising strategy for solving challenging applications in the field of PLM, such as light-harvesting and composition for new greenhouse installations, which would have a grid consumption to obtain light for photosynthesis processes.

Conflicts of interest

There are no conflicts to declare.

Acknowledgements

The authors thank FAPESP (São Paulo Research Foundation Brazil) (L. C. V. R, process #2018/05280-5, D. L. F, process #2018/26282-6) and CNPq (L. C. V. R., process #315126/2021-3, V. C. T., process #310890/2021-7). The Profs. Koiti Araki and Vera R. L. Constantino are acknowledged for allowing the use of XRD and FTIR. The authors also acknowledge the CNPEM-Sirius facility for the beamtime at Carnaúba Beamline (#20210013) and Eng. Leonardo M. Kofukuda, Eng. Antonio Piccino Neto, Dr Anna Paula S. Sotero, Dr Douglas Galante for the kind assistance during the Synchrotron measurements.

References

1 R. Stefani, L. C. V. Rodrigues, C. A. A. Carvalho, M. C. F. C. Felinto, H. F. Brito, M. Lastusaari and J. Hölsä, *Opt. Mater.*, 2009, **31**, 1815–1818.
2 P. Dorenbos, *J. Electrochem. Soc.*, 2005, **152**, H107.
3 D. O. A. Dos Santos, L. Giordano, M. A. S. G. Barbará, M. C. Portes, C. C. S. Pedroso, V. C. Teixeira, M. Lastusaari and L. C. V. Rodrigues, *Dalton Trans.*, 2020, **49**, 16386–16393.
4 P. Głuchowski, W. Stręk, M. Lastusaari and J. Hölsä, *Phys. Chem. Chem. Phys.*, 2015, **17**, 17246–17252.
5 Z. Pan, Y. Y. Lu and F. Liu, *Nat. Mater.*, 2011, **11**, 58–63.
6 T. Matsuzawa, Y. Aoki, N. Takeuchi and Y. Murayama, *J. Electrochem. Soc.*, 1996, **143**, 2670–2673.
7 R. K. Gartia and N. Chandrasekhar, *Defect Diffus. Forum*, 2014, **357**, 171–191.
8 J. J. Joos, D. Poelman and P. F. Smet, *Phys. Chem. Chem. Phys.*, 2015, **17**, 19058–19078.
9 D. L. Fritzen, L. Giordano, L. C. V. Rodrigues and J. H. S. K. Monteiro, *Nanomaterials*, 2020, **10**, 1–36 art. 2015.
10 D. Poelman, D. Van Der Heggen, J. Du, E. Cosaert and P. F. Smet, *J. Appl. Phys.*, 2020, **128**, 240–903.
11 Y. Zhuang, Y. Katayama, J. Ueda and S. Tanabe, *Opt. Mater.*, 2014, **11**, 1907–1912.
12 C. Ji, J. Tan and Q. Yuan, *Chin. J. Chem.*, 2021, **39**, 3188–3198.
13 L. G. Merízio, E. Bonturim, R. U. Ichikawa, I. G. N. Silva, V. C. Teixeira, L. C. V. Rodrigues and H. F. Brito, *Materialia*, 2021, **20**, 101226.
14 M. Xiong, X. Xi, H. Gong and A. Shui, *J. Sol-Gel Sci. Technol.*, 2017, **81**, 894–902.
15 P. L. Marani, G. D. Bloisi and D. F. S. Petri, *Cellulose*, 2015, **22**, 3907–3918.
16 V. A. Solé, E. Papillon, M. Cotte, P. Walter and J. Susini, *Spectrochim. Acta, Part B*, 2007, **62**, 63–68.
17 M. A. Salim, R. Hussin, M. S. Abdullah, S. Abdullah, N. S. Alias, S. Aishah, A. Fuzi, M. Nor, M. Yusuf and K. M. Mahbor, *Solid State Sci. Technol.*, 2009, **17**, 59–64.
18 S. Villa, P. Riani, F. Locardi and F. Canepa, *Materials*, 2016, **9**, 826.
19 I. P. Sahu, D. P. Bisen, N. Brahme and R. K. Tamrakar, *J. Radiat. Res. Appl. Sci.*, 2015, **8**, 104–109.
20 K. Oksman and R. J. Moon, *Handbook of Green Materials*, 2014, pp. 89–105.
21 D. Van der Heggen, J. J. Joos, D. C. R. Burbano, J. A. Capobianco and P. F. Smet, *Materials*, 2017, **10**, 867.
22 H. F. Brito, J. Hölsä, H. Jungner, T. Laamanen, M. Lastusaari, M. Malkamäki and L. C. V. Rodrigues, *Opt. Mater. Express*, 2012, **2**, 287–293.